Carbon 180 (2021) 197–203

Contents lists available at ScienceDirect

Carbon

journal homepage: www.elsevier.com/locate/carbon

Research Article

Polyacrylonitrile-derived thermally conductive graphite film *via* graphene template effect

Haoguang Huang , Xin Ming , Yazhe Wang , Fan Guo , Yingjun Liu , Zhen Xu , Li Peng **, Chao Gao *

MOE Key Laboratory of Macromolecular Synthesis and Functionalization, Department of Polymer Science and Engineering, Key Laboratory of Adsorption and Separation Materials & Technologies of Zhejiang Province, Zhejiang University, 38 Zheda Road, Hangzhou, 310027, PR China

ARTICLE INFO

Article history:
Received 22 March 2021
Received in revised form
24 April 2021
Accepted 27 April 2021
Available online 11 May 2021

Keywords:
PAN-derived
Graphite film
High crystalline
Thermal conductivity
Flexibility

ABSTRACT

Stable operation of electronic devices requires flexible and thermally conductive graphite film (GF) to spread the locally generated heat in devices. However, the tedious and harsh production procedure, high cost, and brittle nature of commercially available GF derived from polyimide (PI) limited its further applications. Here, we used graphene sheets as a template to induce graphitization of polyacrylonitrile (PAN) in confined 2D space, and thereby generated high crystalline GF. The obtained flexible GF showed a high in-plane thermal conductivity (*K*) of 1282 W m^{-1} K^{-1} and conductivity (σ) of 9.94 × 10^5 S m^{-1}. The *K* *is* 7.3 times than that of pure PAN-derived film, and even higher than pure graphene film (1201 W m^{-1} K^{-1}). Besides, it is easy to produce thick GF (80 μm), which is difficult to achieve in conventional artificial GF. Our work promises low-cost and easy preparation of high-quality GFs from non-graphitizable synthetic and natural macromolecules with the aid of graphene template structure-directing effect.

1. Introduction

With the development of high-power electronic devices, the heat-dissipation efficiency of thermal management materials (TMM) has become a critical concern, which decides the operation reliability and stability of devices [1,2]. GF with high flexibility and thermal conductivity can effectively spread the heat generated locally, especially in devices with complex structures [3,4]. PI-derived GF is one of the most used commercial carbon-based TMM with high thermal conductivity (*K*). While the severe demand on the molecular structure of PI and complex biaxial stretching process undoubtedly increases production cost and decreases manufacturing efficiency [5,6]. Besides, the poor flexibility and uncontrollable thickness of prepared film hinder its application fields.

Recently, much attention has been paid to the newly emerged flexible graphene films that are assembled from graphene oxide (G-O) sheets prepared by chemical approaches. For example, [7–9]. Peng et al. made a defect-free GF with high *K* and flexibility by large-sized G-O sheets. Zhang et al. reported the controllable ultra-thick graphene films based on the self-fusion character between G-O sheets [10]. These researches provided a preparation road to realizing high-quality GF with controlled thickness from G-O. Using G-O as precursors, the rich gas-bags which generated during the thermal annealing process were pressured into micro-folds, which endowed GF with brilliant flexibility [9]. However, the introduction of large-sized G-O greatly increased the cost of raw material due to the complex and low-yield preparation process [7,8]. Meanwhile, the excessive delamination structure and rich micro-folds lowered the thermal stability of graphene films [8–10].

Synergistic crystallization of polymers and graphene sheets was another approach for GF-based TMM [11–17]. For example, Cunning et al. embedded single-crystal graphene layers into SU-8 thin films, resulting in a preferred orientation and graphitization of polymer [18]. This provided theoretical support for the preparation of high-performance composite GF. Wang et al. fabricated a graphite oxide-based film using a 5% ratio of PAN as crosslinkers, and the *K* was improved by 18% owing to the coupling effect of PAN [13]. Wu et al. reported a flexible film fabricated by 4, 4′-diaminodiphenyl ether (ODA, the precursor of PI) grafted graphene oxide. The *in situ* formed PI served as a solder to connect G-O sheets into

* Corresponding author.
** Corresponding author.
E-mail addresses: sspengli@yeah.net (L. Peng), chaogao@zju.edu.cn (C. Gao).

https://doi.org/10.1016/j.carbon.2021.04.090
0008-6223/

large ones and thus enhanced the *K* after a simple thermal treatment [11]. Unfortunately, the *in situ* polymerization process caused a lot of wrinkles on graphene sheets, leading to mass structural defects in the film. Such studies have been limited to the introduction of a polymer as crosslink fillers, in strong contrast to our use of PAN as a carbon precursor to prepare GF.

Herein, we used graphene sheets as a template to induce graphitization of PAN in confined 2D space, and thereby generate high crystalline GF. The structure-directing effect of graphene on the carbonization and graphitization of polymer was studied in detail. Moreover, linear polymers exhibited ultra-high chemical activity at high temperatures, facilitating the transition of the AB stacking structure. Therefore, the PAN-derived GF with 50% contents of G-O showed a high in-plane *K* of 1282 W m^{-1} k^{-1}, σ of 9.94 × 10^5 S m^{-1}, even higher than pure graphene film (1201 W m^{-1} k^{-1}). Meanwhile, the good flexibility of this GF was maintained as graphene films due to the nearly 100% graphitization of sp^3 carbon in PAN and generation of appropriate delamination structures. The demonstrated self-fusion effect of graphene was also suitable for composite materials, tuning the thickness of GF from 4 to 80 μm.

2. Experimental

2.1. Preparation of PAN-derived GF

N, *N*-Dimethylacetamide (DMAc) dispersion of G-O sheets with a large lateral size of 25–35 μm was purchased from Hangzhou Gaoxi Technology Co. Ltd. The PAN was got from Shanghai Dibai Biological Co., Ltd. The PAN was dispersed in DMAc solution with a mass fraction of 10%. To prepare composite films, the G-O and PAN were mixed with different mass fractions, then, mixed uniformly and removed the air bubbles to obtain the mixture. The mixed slurry was coated on PET films with a thickness of 2–5 mm, followed by drying at 60 °C in the drying oven. The obtained films were hot-press in the air with the temperature rise to 270 °C for 2 h. Finally, the films were gradually annealed to 2800 °C to prepare PAN-derived GF. Before characterization, these films were pressed under pressure of 300 MPa. The dried films were annealed to a different temperature to observe the preparation mechanism, including 270 °C, 2000 °C, 2300 °C. The G-O films were immersed in hydroiodic acid for 12 h at 90 °C to obtain rG-O.

2.2. Preparation of PAN-derived thick film

Several dried films were immersed in DMAc solution for 10 min. The swollen films were stacked together and dried in air at 90 °C to get thick composite films. Then, the films were heated at 270 °C under a pressure of 10 MPa, followed by a 2800 °C high-temperature annealing protected by argon. Finally, the thick and densified composite film was obtained after a 300 MPa pressing for 12 h.

2.3. Characterization

Morphologies of the films were observed by a field emission scanning electron microscope (SEM, Hitachi S4800) at 5 kV. The lattice of the GFs was observed by a transmission electron microscope (TEM, Hitachi H-9500). Thermal conductivity was tested by laser flash method using NanoFlash instrument (Netzsch LFA 467). The electrical conductivity was evaluated by a four-probe method using a Keithley 2460 source meter. Raman spectroscopy was performed by a commercial Renishaw in Via-Reflflex Raman microscopy at an excitation wavelength of 532 nm. XRD was measured on an X'Pert PRO diffractometer (PANalytical) using Cu Ka1 radiation with an X-ray wavelength of 1.5406 Å.

3. Results and discussion

The composite film containing PAN and single-layer G-O was prepared by the solution casting method (Fig. 1a). The dried film was annealed at 270 °C for pre-oxidation of PAN. During this process, a 0.5 MPa pressure was applied to ensure the smoothness of the film. After a 2800 °C treatment, the PAN-derived GF was obtained. Fig. 1b–e schematically showed the structural evolution of the film before and after 2800 °C annealing. For pure PAN film, the molecular chain of PAN is oriented in three-dimensional spaces (Fig. 1b). The diffraction ring in the selected area electron diffraction (SAED) pattern suggests the amorphous crystallization of PAN after thermal treatment (Fig. 1c and Figs. S1a–c). When PAN was confined in the interlayer of graphene, the obtained PAN-derived GF exhibits a high crystalline structure, as confirmed by the SAED pattern (Fig. 1e and Fig. S1j-l) [19–21].

To further investigate the structural evolution of the PAN in confined 2D space, the cross-sectional High-resolution TEM (HR-TEM) images of GFs with different ratios of PAN and G-O were analyzed (Fig. S1). After annealing at 2800 °C, the structure of the PAN film shows a random orientation (Fig. 2a). The interlayer spacing of the crystalline domain (*d*-spacing) was 0.38 ± 0.002 nm [18]. Interestingly, an ordered orientation was formed when 10% G-O was added. The crystallization degree of GF increased with G-O contents (Fig. 2b–d). When the G-O content increased to 50%, the *d*-spacing of the film was reduced to 0.337 ± 0.002 nm, similar to that of ideal graphite [22]. The *d*-spacing in the TEM image is calculated as: dotted box distance/number, showing a reduced trend with enhancement of G-O contents.

XRD patterns were performed to trace the structural evolution of PAN-derived GF at different temperatures (Fig. 2e–h). At 270 °C, the PAN film exhibits a peak at 17° (2θ, Fig. 2e), corresponding to the diffraction of the (100) planes [23]. While the (100) peak disappears and the (002) peak of graphene emerges at 25° when added 10% content of G-O [24]. This phenomenon suggests that 10% G-O disrupts the original orientation of PAN, inducing them aligned along with the G-O template.

These films were then annealed to 2800 °C (Fig. 2f). The XRD patterns of PAN film exhibit a diffraction peak at 2θ = 25.9° with a full width at half maximum (FWHM) of 1.232°. In contrast, a higher value of 2θ (26.3°) and narrower FWHM (0.40°) are obtained in the PAN-derived GF contained 10% contents of G-O [18], suggesting a better crystallization structure achieved in the G-O induced PAN layer films. As G-O content increases, the peak position gradually moves to 26.5°, the FWHM decreases to 0.25° and *d*-spacing reduces to 0.335 nm until the G-O content increased to 50% (Fig. 2g). These results are consistent with the analysis of TEM data. Meanwhile, the crystallite thickness (Lc) increases from 6.5 nm to 31 nm (Fig. 2h), which demonstrates that this ratio of G-O gives the best structure-directing effect to induce graphitization of PAN (Fig. S2).

As shown in the Raman spectra (Fig. 2i), the I_D/I_G value of PAN-derived GF (0.18) is decreased to 0 with a 50% ratio of G-O added in the GF, also confirming the reduced structural defects by structure-directing of graphene. Moreover, with the increase of G-O content, the structure-directing effect of graphene is enhanced (Fig. S3). The crystallite dimensions (La) increases from 0.13 μm to 4.86 μm (Fig. 2j), indicating that the graphene sheet can promote lattice growth of PAN during the graphitization process.

The GF with a G-O content of 50% obtained the highest AB stacking order, observing from the 2D peak of Raman spectra (Fig. 2i). When G-O content is lower than 50%, the intensity of the $2D_2$ peak (2720 cm^{-1}, breath vibration of AB structure) is improved with the decrease of structure defects (D peak, 1342.5 cm^{-1}). This

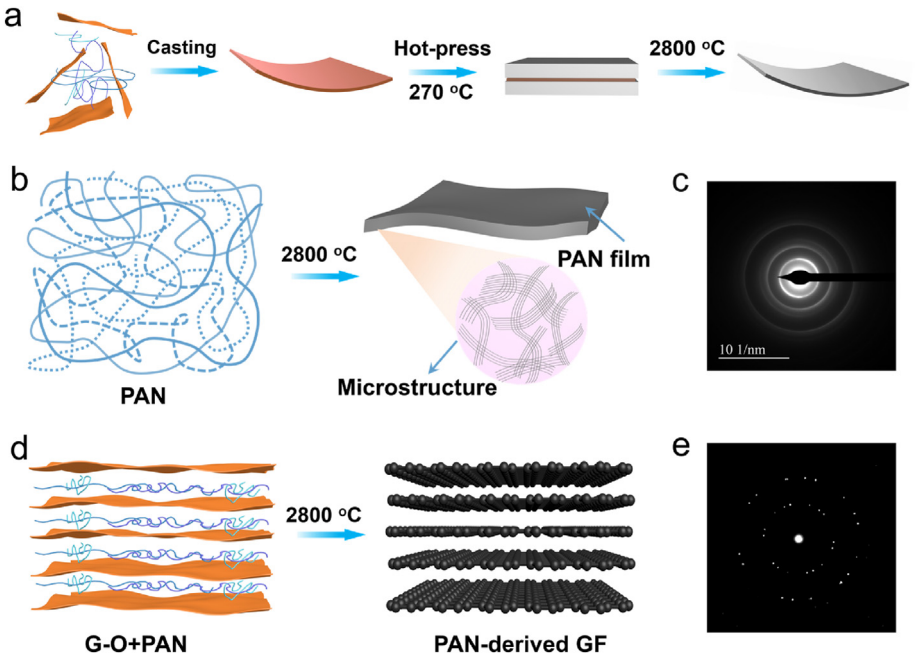

Fig. 1. (a) The preparation process of PAN-derived GF. (b) The schematic diagram for the structural evolution of PAN film after 2800 °C annealing. (c) SAED pattern of pure PAN film after 2800 °C annealing. (d) The schematic diagram for the structural evolution of PAN-derived film after 2800 °C annealing. (e) SAED pattern of PAN-derived film after 2800 °C annealing. (A colour version of this figure can be viewed online.)

demonstrates the PAN has a positive role on graphene, which can promote the transition of AB stacking order of the films due to its strong chemical activity at high-temperature [25–27]. However, when G-O content is higher than 50%, the $2D_2$ peak is slightly decreased. This is because that mass discontinuous crystals are formed in the interlayer of graphene with the decrease of PAN content, increasing edge defects and thus weakening the AB stacking degree.

SEM images illustrated the micromorphology of PAN-derived films before and after 2000, 2300 and 2800 °C annealing (Fig. 3a–h and Figs. S4–5). The pure PAN film becomes a carbon block without orientation (Fig. 3a). When 10% contents of G-O are added, the layered structure appears in the composite film (Fig. 3b). After that, the layered structure maintains and even becomes obvious with the increase of the G-O ratio (Fig. 3c and d). After 2800 °C annealing, no obvious changes in the orientation are found in the pure PAN films (Fig. 3e). In contrast, a clear layered structure of the PAN-derived film is shown with the G-O ratio increased to 10%, suggesting preferential orientation of linear PAN molecules along with the graphene sheets [28]. When the G-O content reaches 50%, arched structures appear between the graphene layers, which gradually develop into micro-gasbags with the increase of G-O content. Although the micro-gasbags would contribute to the flexibility of GF, they lower thermal stability and enhance the interface phonon scattering of the film. While in the case of PAN-derived GF, the rich defects of polymers act as gas-escaping channels during the thermal treatment process, inhibiting the generation of micro-gasbags (Fig. S6). Combing the XRD and Raman results (Fig. 2f and S7), the PAN-derived GF with a 50% ratio of G-O realizes a high degree of graphitization and orientation, which lays a solid structural foundation for higher thermal conductivity.

We evaluated the performances of the PAN-derived film by density, in-plane *K*, and σ, which have similar variation trends. When the G-O ratio is lower than 30%, low density (less than 1.2 g cm^{-3}), poor conductive properties (including *K* and σ) are shown due to incomplete graphitization of sp^3 carbons in PAN. When G-O content reaches 30%, the density, *K*, and σ of the films is 1.9–2.0 g cm^{-3}, 1089 W m^{-1} $K^{-1,}$ and 9.5 × 10^5 S m^{-1}, respectively (Fig. 3j and k), benefiting from the good structure-directing effect of graphene. With the healing of structural defects, we get the optimized *K* (1282 W m^{-1} k^{-1}) and σ (9.94 × 10^5 S m^{-1}) by PAN-derived GF with a G-O ratio of 50%. After that, mass generated micro-gasbags enhance phonon scattering and reduce the *K* of these films [29,30].

The PAN showed a repair effect to graphene, which helped to heal the atomic defects on G-O sheets and improved the stacking order of GF (Fig. 4a). We compared the repairing effect of PAN-derived GF with 50% contents of G-O, chemical reduction G-O (rG-O), and pure G-O [31,32]. After a 2000 °C treatment, the rG-O shows a smaller I_D/I_G (0.017) than that of G-O (0.029) due to the lower content of holes (Fig. 4b). Interestingly, the I_D/I_G of PAN-derived GF (0.014) is even lower than that of rG-O, indicating that the carbon atoms in PAN can repair defects in the graphene sheet under the temperature of 2000 °C (Fig. 4b). Furthermore, the PAN-derived GF exhibits a higher value (71%) of AB stacking order than that of G-O (18%) and rG-O (46%) after 2300 °C annealing [33–35]. This result confirms that PAN in high temperature shows high chemical activity, promoting the AB transformation of graphene films (Fig. 4c).

Thanks to the structure-directing effect of graphene, the PAN-derived films with a 50% ratio of G-O show a transformation from amorphous carbon (270 °C) to a highly crystalline structure (Fig. 4d–f). The highly oriented lattice fringes with a *d*-spacing of 0.36 nm indicate that the amorphous carbons are transferred into twisted graphene sheets (Fig. 4e). When the temperature rises to 2300 °C, the *d*-spacing of the film is further reduced to 0.338 nm (Fig. 4f), which is consistent with the strong $2D_2$ peak in Fig. 4c.

We then evaluated the morphology and flexibility of PAN and PAN-derived GF with a 50% ratio of G-O. As shown in Fig. 5a, The PAN film is transparent and flexible but becomes fragile after annealed at 2800 °C (Fig. 5a and b). The PAN-derived GF remains intact and shows flexibility when treated at 2800 °C, which can be

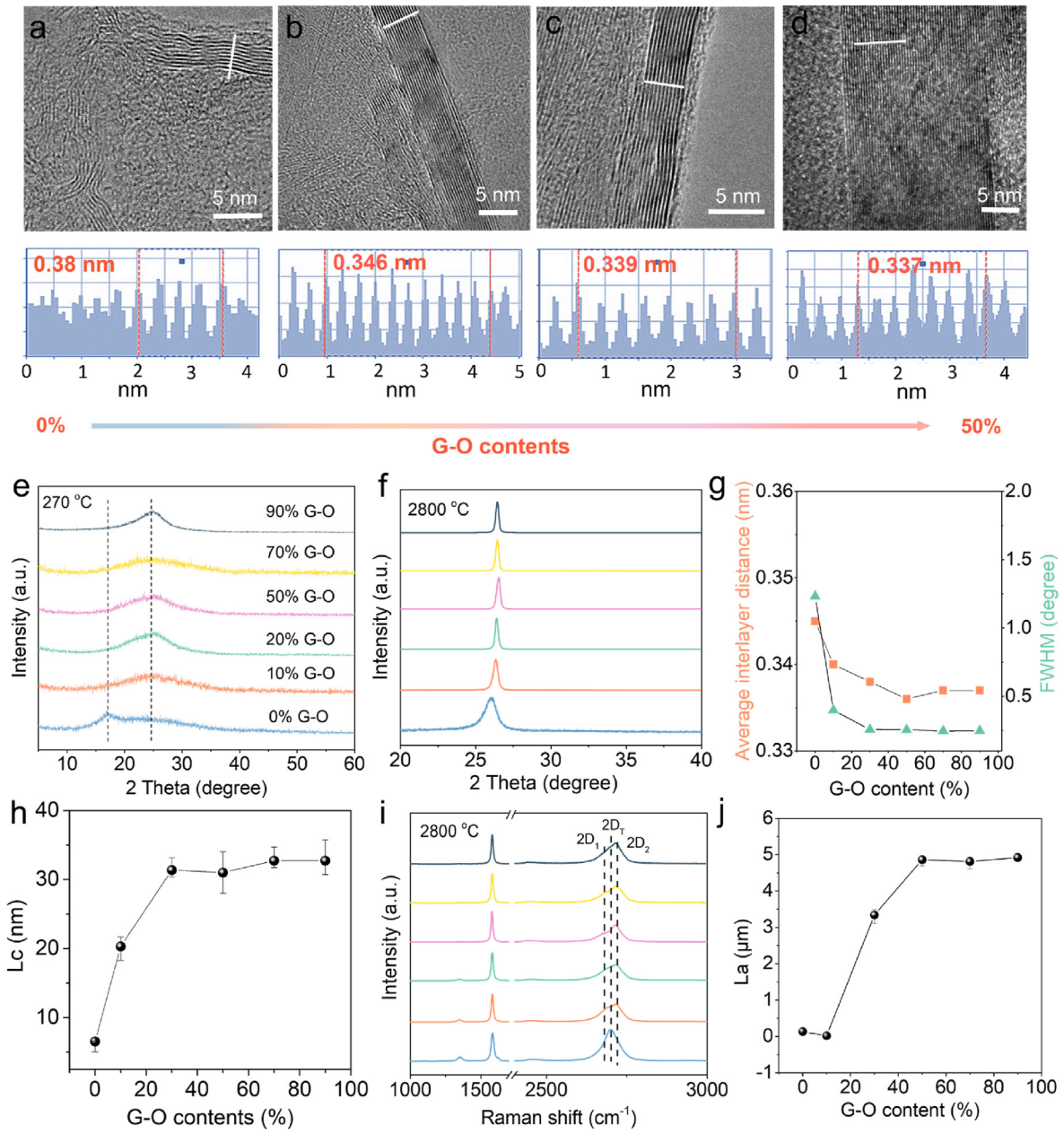

Fig. 2. (a–d) Cross-sectional HR-TEM images and corresponding intensity line profiles of the PAN-derived GFs with 0% G-O (a), 10% G-O (b), 30% G-O (c), and 50% G-O (d) after annealed at 2800 °C. (e–f) XRD of the PAN-derived films annealed at (e) 270 °C and (f) 2800 °C. (g) FWHM and *d*-spacing of the PAN-derived GFs from (f). (h) Crystallite thickness (Lc) of the PAN-derived GFs from (f). (i) Raman spectra of PAN-derived GFs annealed at 2800 °C. The 2D peak is fitted with 3 Lorentzian peaks: $2D_1$ (~2680 cm^{-1}) and $2D_2$ (~2720 cm^{-1}) for AB stacked graphite and $2D_T$ (~2700 cm^{-1}) for turbostratic graphite. (j) Crystallite dimensions (La) of the PAN-derived GFs from (i). (A colour version of this figure can be viewed online.)

folded into a crane (Fig. 5c–e). The film can endure 180° bending as shown in Fig. 5f. The conductivity of GF hardly decreased during 5000 times bending cycles, confirming the good flexibility of the GF (Fig. 5g). Furthermore, we controlled the thickness of PAN-derived GF from 3 μm to 80 μm by the self-fusion effect of graphene [10]. As shown in the SEM images (Fig. 5h–k), the increase of thickness does not have an obvious influence on the orientation structure of the films, and thus the *K*. Furthermore, the structure-directing effect of graphene can extend to other polymers (such as lignin, PI), which induces polymers to be macroscopic GFs (Fig. S8).

4. Conclusion

In conclusion, the structure-directing effect of graphene on the carbonization and graphitization of PAN within the macro-assembled films was observed. By embedding single-layer G-O sheets in PAN film, we prepared highly crystalline and flexible GF. With adding of 50% G-O, the PAN-derived film shows a defect-free and highly ordered AB stacking structure with a *d*-spacing of 0.336 nm. The GF shows a high conductivity (9.94×10^5 S m^{-1}) and in-plane *K* (1282 W m^{-1} k^{-1}). Given the self-fusion effect of the G-O, the thickness of the films can be tuned from 3 to 80 μm. This method not only realizes the preparation of high-performance

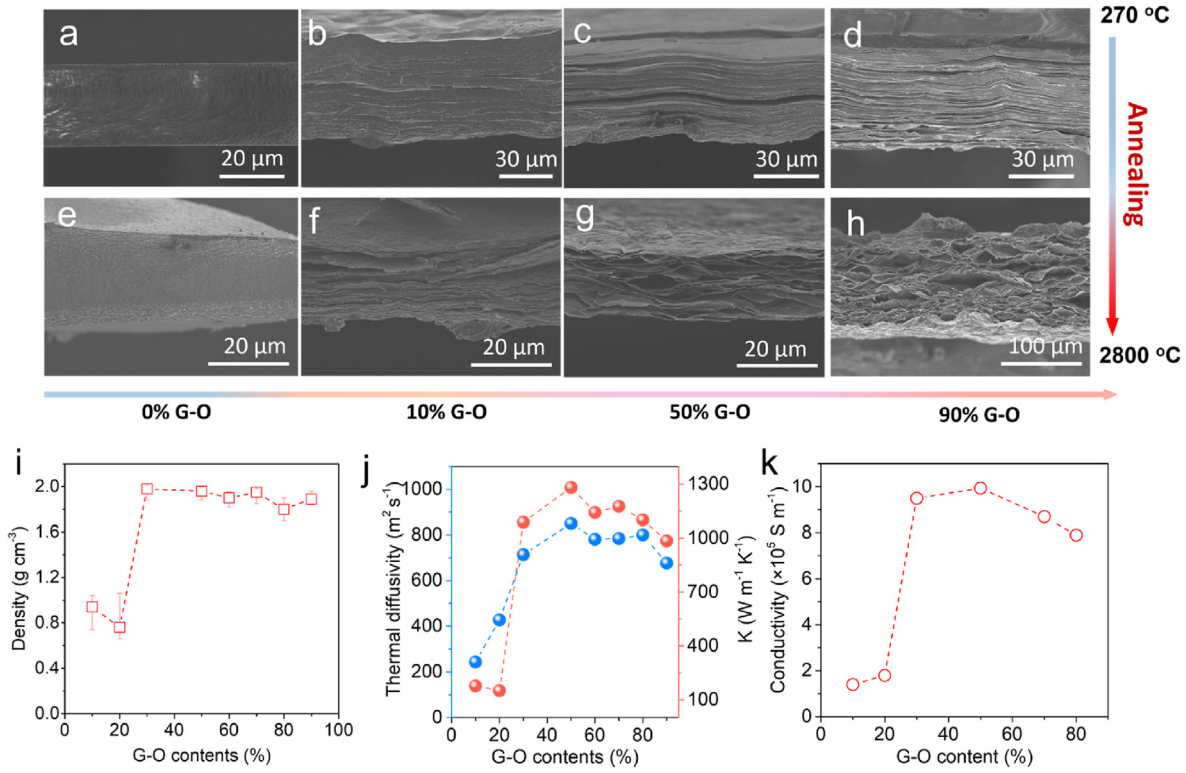

Fig. 3. (a–d) Cross-sectional SEM images of PAN-derived films annealed at 270 °C. (e–h) Cross-sectional SEM images of PAN-derived GFs annealed at 2800 °C. (i) The density of the different ingredient PAN-derived GFs. (j) Thermal diffusivity and conductivity of the different ingredient PAN-derived GFs. (k) Conductivity of the different ingredient PAN-derived GFs. (A colour version of this figure can be viewed online.)

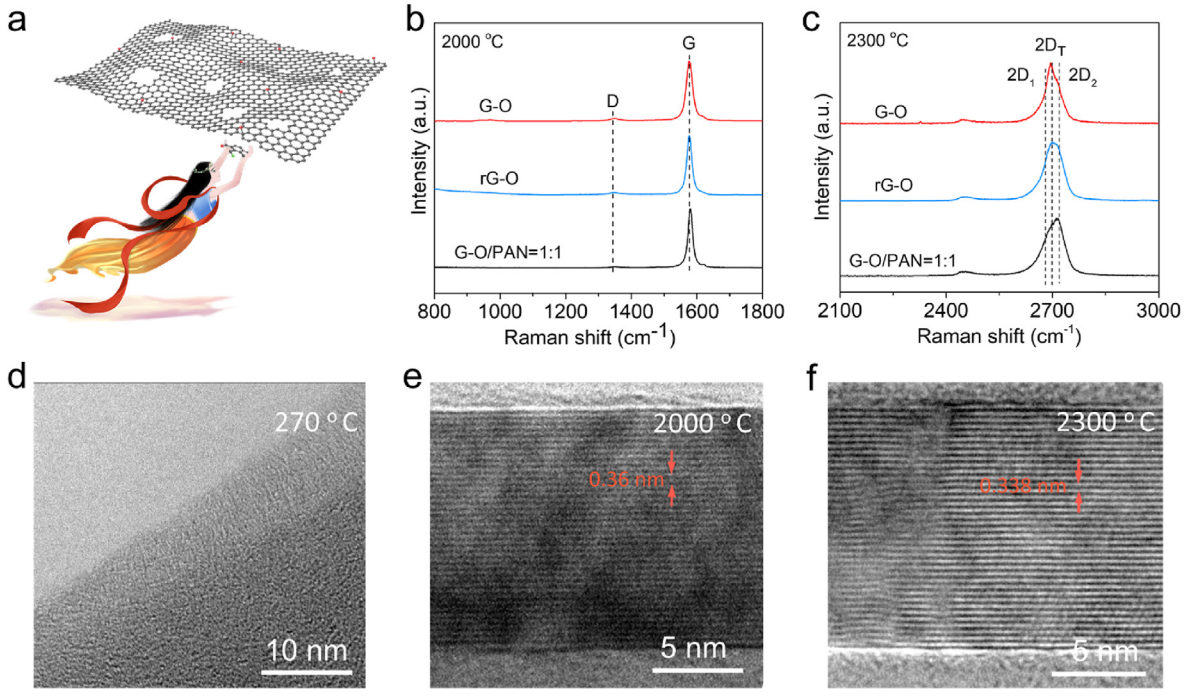

Fig. 4. (a) Schematic diagram for the repair effect of PAN towards graphene. (b) Raman spectra of G-O, rG-O, PAN-derived GF with 50% G-O annealed at 2000 °C. (c) Raman spectra of G-O, rG-O, PAN-derived GF with 50% G-O annealed at 2300 °C. The 2D peak is fitted with 3 Lorentzian peaks: $2D_1$ (~2680 cm^{-1}) and $2D_2$ (~2720 cm^{-1}) for AB stacked graphite and $2D_T$ (~2700 cm^{-1}) for turbostratic graphite. (d–f) TEM images of PAN-derived GFs with 50% G-O annealed after 270 °C, 2000 °C, 2300 °C, respectively. (A colour version of this figure can be viewed online.)

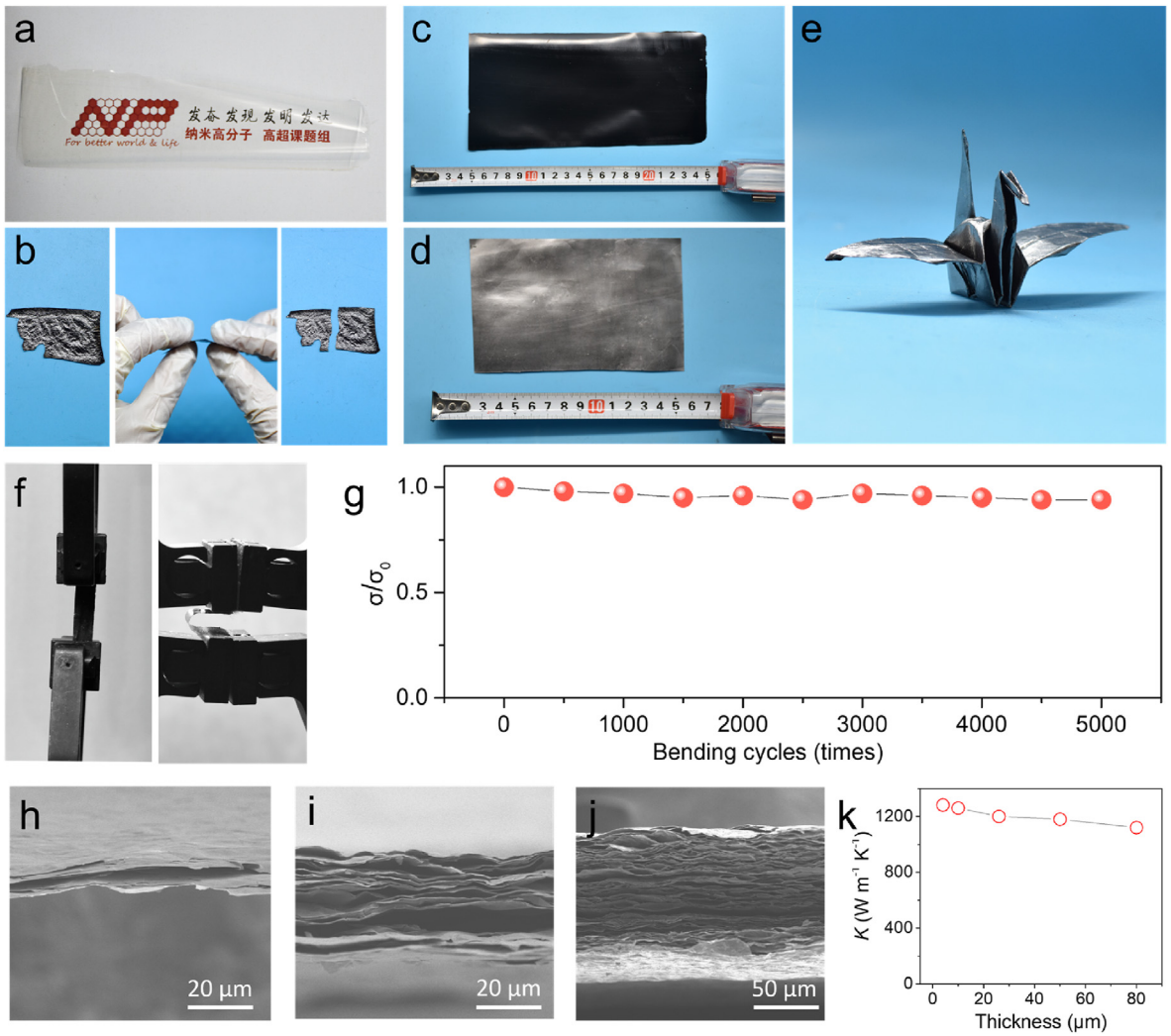

Fig. 5. (a) PAN film. (b) PAN film after annealing at 2800 °C. (c) PAN-derived film. (d) PAN-derived GF. (e) A crane made by PAN-derived GF. (f) The bending test of PAN-derived GF. (g) Conductivity variation under cyclic bending for 5000 times. (h–j) PAN-derived GF with different thicknesses. (k) The thermal conductivity of PAN-derived GF with different thicknesses (G-O contents in these PAN-derived GF is 50%). (A colour version of this figure can be viewed online.)

macroscopic polymer-based GF but also gives guidance for the graphitization of polymers. Further, this simple strategy provides a prospect for the industrial preparation of high thermal conductive yet flexible GF at a low-cost.

CRediT authorship contribution statement

Haoguang Huang: Conceptualization, Methodology, Investigation, Data curation, Formal analysis, Visualization, Writing – original draft. **Xin Ming:** Validation. **Yazhe Wang:** Investigation, Project administration. **Fan Guo:** Investigation, Formal analysis. **Yingjun Liu:** Writing – review & editing, Validation. **Zhen Xu:** Funding acquisition, Supervision. **Li Peng:** Supervision, Conceptualization, Writing – review & editing, Funding acquisition. **Chao Gao:** Supervision, Conceptualization, Writing – review & editing, Funding acquisition.

Declaration of competing interest

The authors declare that they have no known competing financial interests or personal relationships that could have appeared to influence the work reported in this paper.

Acknowledgment

This work is supported by the National Key R&D Program of China (No. 2016YFA0200200), National Natural Science Foundation of China (Nos. 51803177, 51533008, 51703194, 51603183, 21805242), Fundamental Research Funds for the Central Universities (No. 2017QNA4036), Hundred Talents Program of Zhejiang University (188020*194231701/113), the key research and development plan of Zhejiang Province (2018C01049), the National Postdoctoral Program for Innovative Talents (BX201700209), and the China Postdoctoral Science Foundation (2017M620241 and 2020M681819).

Appendix A. Supplementary data

Supplementary data to this article can be found online at https://doi.org/10.1016/j.carbon.2021.04.090.

References

[1] W. Lee, K. Kim, W. Jeong, L.A. Zotti, F. Pauly, J.C. Cuevas, et al., Heat dissipation in atomic-scale junctions, Nature 498 (2013) 209–212.
[2] N. Han, T.V. Cuong, M. Han, B.D. Ryu, S. Chandramohan, J.B. Park, et al.,

Improved heat dissipation in gallium nitride light-emitting diodes with embedded graphene oxide pattern, Nat. Commun. 4 (2013) 1452.
[3] A. Akbari, B.V. Cunning, S.R. Joshi, C. Wang, D.C. Camacho-Mojica, S. Chatterjee, et al., Highly ordered and dense thermally conductive graphitic films from a graphene oxide/reduced graphene oxide mixture, Matter 2 (2020) 1–9.
[4] M. Murakami, A. Tatami, M. Tachibana, Fabrication of high quality and large area graphite thin films by pyrolysis and graphitization of polyimides, Carbon 145 (2019) 23–30.
[5] M. Murakami, K. Watanabe, S. Yoshimura, High-quality pyrographite films, Appl. Phys. Lett. 48 (23) (1986) 1594–1596.
[6] H. Hatori, Y. Yamada, M. Shiraishi, In-plane orientation and graphitizability of polyimide films: II. Film thickness dependence, Carbon 31 (1993) 1307–1312.
[7] D. Akinwande, N. Petrone, J. Hone, Two-dimensional flexible nanoelectronics, Nat. Commun. 5 (2014) 5678.
[8] K.S. Novoselov, V.I. Fal'ko, L. Colombo, P.R. Gellert, M.G. Schwab, K.A. Kim, Roadmap for graphene, Nature 490 (2012) 192–200.
[9] L. Peng, Z. Xu, Z. Liu, Y. Guo, P. Li, C. Gao, Ultrahigh thermal conductive yet superflexible graphene films, Adv. Mater. 29 (2017) 1700589.
[10] X. Zhang, Y. Guo, Y. Liu, Z. Li, W. Fang, L. Peng, et al., Ultrathick and highly thermally conductive graphene films by selffusion, Carbon 167 (2020) 249–255.
[11] X. Wu, H. Li, K. Cheng, H. Qiu, J. Yang, Modified graphene/polyimide composite films with strongly enhanced thermal conductivity, Nanoscale 11 (2019) 8219–8225.
[12] Y. Zhu, Q. Peng, Y. Qin, X. Zhao, L. Xu, Q. Chen, Graphene–Carbon composite films as thermal management materials, ACS Appl. Nano Mater. 3 (2020) 9076–9087.
[13] K. Wang, M. Li, J. Zhang, H. Lu, Polyacrylonitrile coupled graphite oxide film with improved heat dissipation ability, Carbon 144 (2019) 249–258.
[14] A. Koganemaru, Y. Bin, H. Tohora, F. Okino, S. Komiyama, J. Zhu, et al., Carbonization of oriented polyacrylonitrile and multiwalled carbon nanotube composite films, Asia-Pac, J. Chem. Eng. 3 (2008) 521–526.
[15] J.L. Suter, R.C. Sinclair, P.V. Coveney, Principles governing control of aggregation and dispersion of graphene and graphene oxide in polymer melts, Adv. Mater. 32 (2020) 2003213.
[16] H.G. Chae, M.L. Minus, A. Rasheed, S. Kumar, Stabilization and carbonization of gel spun polyacrylonitrile/single wall carbon nanotube composite fibers, Polymer 48 (2007) 3781–3789.
[17] H. Chang, Y. Jia, L. Xiao, H. Chen, K. Zhao, Y. Chen, et al., Three dimensional cross-linked and flexible graphene composite paper with ultrafast electro-thermal response at ultra-low voltage, Carbon 154 (2019) 150–155.
[18] B.V. Cunning, B. Wang, T.J. Shin, R.S. Ruoff, Structure-directing effect of single crystal graphene film on polymer carbonization and graphitization, Mater. Horiz. 6 (2019) 796–801.
[19] T. Kyotani, N. Sonobe, A. Tomita, Formation of highly orientated graphite from polyacrylonitrile by using a two-dimensional space between montmorillonite lamellae, Nature 311 (1988) 331–333.
[20] F. Jiang, Y. Yao, B. Natarajan, C. Yang, T. Gao, H. Xie, et al., Ultrahigh temperature conversion of biomass to highly conductive graphitic carbon, Carbon 144 (2019) 241–248.
[21] H. Hatori, Y. Yamada, M. Shiraishi, In-plane orientation and graphitizability of polyimide films, Carbon 30 (1992) 763–766.
[22] S.B. Austerman, S.M. Myron, J.W. Wagner, Growth and characterization of graphite single crystals, Carbon 5 (1967) 549–557.
[23] Y. Zhang, N. Tajaddod, K. Song, M.L. Minus, Low temperature graphitization of interphase polyacrylonitrile (PAN), Carbon 91 (2015) 479–493.
[24] G. Xin, H. Sun, T. Hu, H.R. Fard, X. Sun, et al., Large-area freestanding graphene paper for superior thermal management, Adv. Mater. 26 (2014) 4521–4526.
[25] H. Huang, L. Peng, W. Fang, S. Cai, X. Chu, Y. Liu, et al., A polyimide-pyrolyzed carbon waste approach for the scalable and controlled electrochemical preparation of size-tunable graphene, Nanoscale 12 (2020) 11971–11978.
[26] D. Papkov, A. Goponenko, O.C. Compton, Z. An, A. Moravsky, X.Z. Li, et al., Improved graphitic structure of continuous carbon nanofibers via graphene oxide templating, Adv. Funct. Mater. 46 (2013) 5763–5770.
[27] N.R. Wilson, P.A. Pandey, R. Beanland, R.J. Young, I.A. Kinloch, L. Gong, et al., Graphene oxide: structural analysis and application as a highly transparent support for electron microscopy, ACS Nano 3 (2009) 2547–2556.
[28] B. Saha, A.O. Furmanchuk, Y. Dzenis, G.C. Schatz, Multi-step mechanism of carbonization in templated polyacrylonitrile derived fibers: ReaxFF model uncovers origins of graphite alignment, Carbon 94 (2015) 694–704.
[29] P. Kumar, F. Shahzad, S. Yu, S.M. Hong, Y.-H. Kim, C.M. Koo, Large-area reduced graphene oxide thin film with excellent thermal conductivity and electromagnetic interference shielding effectiveness, Carbon 94 (2015) 494–500.
[30] R. Rozada, J.I. Paredes, S. Villar-Rodil, A. Martínez-Alonso, J.M.D. Tascón, Towards full repair of defects in reduced graphene oxide films by two-step graphitization, Nano Res. 6 (2013) 216–233.
[31] S. Pei, J. Zhao, J. Du, W. Ren, H.-M. Cheng, Direct reduction of graphene oxide films into highly conductive and flexible graphene films by hydrohalic acids, Carbon 48 (2010) 4466–4474.
[32] I.K. Moon, J. Lee, R.S. Ruoff, H. Lee, Reduced graphene oxide by chemical graphitization, Nat. Commun. 1 (2010) 1.
[33] A.C. Ferrari, Raman spectroscopy of graphene and graphite: disorder, electron–phonon coupling, doping and nonadiabatic effects, Solid State Commun. 143 (2007) 47–57.
[34] L.G. Cançado, K. Takai, T. Enoki, M. Endo, Y.A. Kim, H. Mizusaki, et al., Measuring the degree of stacking order in graphite by Raman spectroscopy, Carbon 46 (2) (2008) 272–275.
[35] B. Wang, B.V. Cunning, N.Y. Kim, F. Kargar, S.-Y. Park, Z. Li, Ultrastiff, strong, and highly thermally conductive crystalline graphitic films with mixed stacking order, Adv. Mater. 31 (2019) 1903039.